Nazemi, A., He, X., MacFarlane, L., Harniman, R., Hsiao, M-S., Winnik, M., Faul, C. FJ., & Manners, I. (2017). Uniform “Patchy” Platelets by Seeded Heteroepitaxial Growth of Crystallizable Polymer Blends in Two Dimensions. *Journal of the American Chemical Society*, *139*(12), 4409–4417. https://doi.org/10.1021/jacs.6b12503

Uniform "Patchy" Platelets by Seeded Heteroepitaxial Growth of Crystallizable Polymer Blends in Two Dimensions

Ali Nazemi,[†] Xiaoming He,[†,§] Liam R. MacFarlane,[†,§] Robert L. Harniman,[†] Ming-Siao Hsiao,[‡] Mitchell A. Winnik,[∥] Charl F.J. Faul,[†] and Ian Manners[*,†]

[†]School of Chemistry, University of Bristol, Bristol BS8 1TS, United Kingdom

[‡]UES, Inc. and Materials & Manufacturing Directorate, Air Force Research Laboratory, Wright-Patterson AFB, OH 45433, USA

[∥]Department of Chemistry, University of Toronto, Toronto, Ontario M5S 3H6, Canada

ABSTRACT: Rectangular platelets formed by the self-assembly of block copolymers in selective solvents are of interest for a range of applications. Recently we showed that the seeded growth of crystallizable blends of a block copolymer and homopolymer yields well-defined, low dispersity examples of these two-dimensional (2D) structures. The key feature was the use of the same crystallizable polymer segment in the seed and blend components to enable an efficient homoepitaxial growth process. Herein we demonstrate that this 2D crystallization-driven self-assembly approach can be extended to *heteropitaxial* growth by the use of different crystallizable polymers with compatible crystal structures. This allows the formation of well-defined "patchy" rectangular platelets and platelet block comicelles with different core chemistries. The use of scanning transmission electron microscopy–energy-dispersive X-ray spectroscopy provided key information on the spatial location of the components in the resulting assemblies and thereby valuable insight into the 2D heteroepitaxial growth process.

INTRODUCTION

Nanoscale two-dimensional (2D) polymer-based platelet structures are of considerable interest for a range of applications from composite reinforcement to liquid crystals.[1] For example, platelets formed by crystallizable homopolymers, such as thiol-functionalized poly(ethylene oxide) (PEO) and polycaprolactone (PCL) can be used as platforms for nanoparticle attachment and patterning.[2] Using this approach, PEO sheets with programmable patterns including binary magnetite nanoparticles/semiconducting quantum dots and gold nanoparticles have been prepared.[3] The self-assembly of block copolymers (BCPs) in selective solvents represents another possible route to platelets. However, BCPs with amorphous core-forming segments rarely form this morphology, and generally yield spherical micelles or core-shell nanoparticles with a variety of other shapes such as worm-like micelles,[4] toroids,[5] and vesicles,[6] as well as more complex, kinetically-trapped morphologies.[7] In contrast, the use of BCPs with a crystallizable core-forming block tends to favour the formation of micelles with low curvature of the core-corona interface, a process termed crystallization-driven self-assembly (CDSA).[8-10] 2D platelets are commonly formed from relatively symmetric BCPs[8,9] whereas one-dimensional (1D) cylindrical or fiber-like micelles are favored for unsymmetrical BCPs with significantly longer corona-forming blocks.[10]

Several significant further advances have been reported in terms of the formation of well-defined and complex platelet architectures from BCPs. For example, alternating rings of BCP and homopolymer have been created by the addition of homopolymer solution to preformed BCP platelets.[9a,9b] We have applied seeded-growth strategies previously developed[11,12] for the formation of uniform and complex 1D cylindrical micelles, termed "living CDSA", to the formation of platelets. For example, addition of near symmetrical BCPs with a crystallizable poly(ferrocenyldimethylsilane) (PFDMS)[13] core-forming block to small seed micelles, generated from the sonication of cylindrical PFDMS BCP micelles with a long corona-forming block, yielded near-uniform lenticular platelets.[14] The area was controlled by the ratio of the seed to added BCP in a process analogous to a living polymerization of covalent monomers except in 2D. Furthermore, sequential addition of different PFDMS BCPs led to the formation of lenticular platelet block comicelles containing spatially-defined regions with different coronal chemistries.[14] A similar 2D seeded growth process has also been reported for hyperbranched poly(ether amine) capped with a polyhedral oligomeric silsesquioxane by Jiang and coworkers.[15]

Recently, we demonstrated that well-defined rectangular platelets can be obtained by the seeded-growth of crystallizable polymer blends of an unsymmetrical PFDMS BCP and PFDMS homopolymer to a solution of

cylindrical seed micelles.[16,17] This process also proceeds as a living 2D CDSA process and provides access to low dispersity samples of platelets with area control. Moreover, rectangular platelet multiblock comicelles and the corresponding hollow structures were obtained by the sequential addition of blends with different corona-forming blocks and the use of crosslinking/dissolution strategies.[16] These living CDSA processes result from homoepitaxial growth of the PFDMS segments of the added BCP and homopolymer from pre-existing seed cores or platelet edges that consist of single crystalline PFDMS.[18]

Scheme 1. General schematic representation of platelet and platelet block comicelle formation discussed in this paper. All self-assembly experiments were carried out in 1:1 (v/v) EtOAc/*i*-PrOH at 45°C.

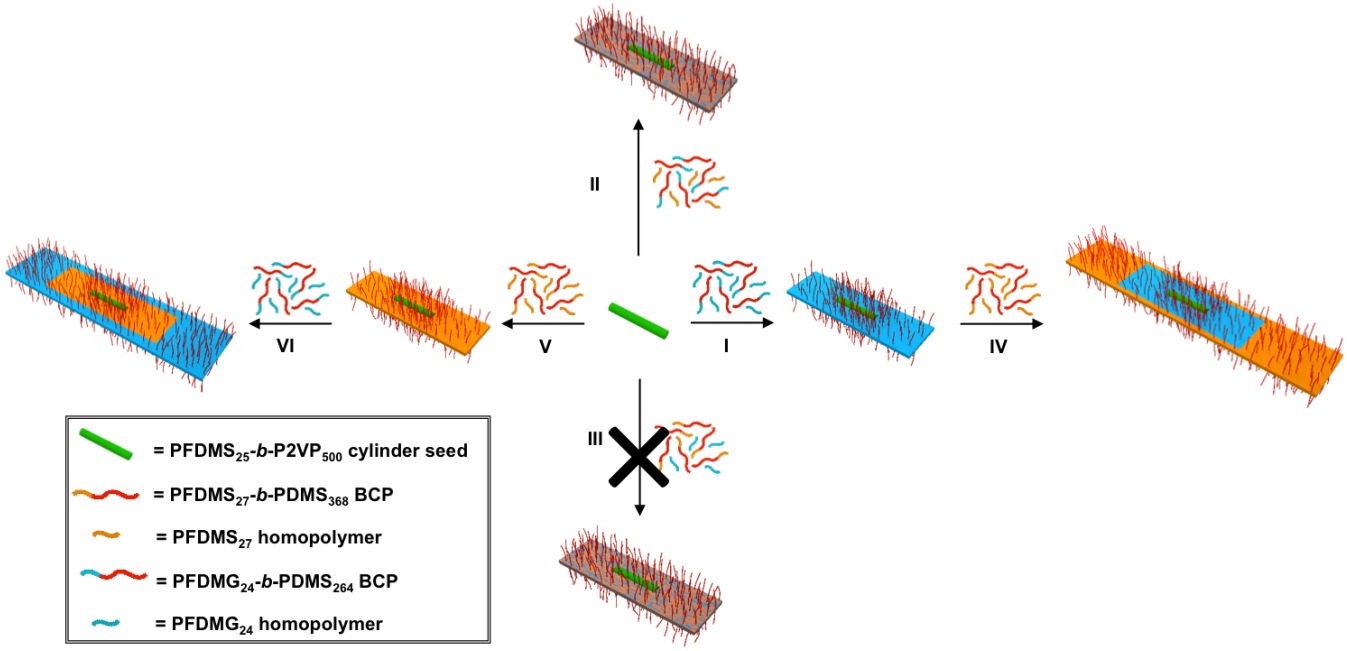

The ability to perform 2D *heteroepitaxial* living CDSA would be expected to represent a significant advance with respect to tailoring platelets as it would allow the creation of spatially-distinct regions with different core structures. A key requirement for heteroepitaxial growth is that the packing of the different crystalline components is similar. Such processes have been observed in 1D for cylinders[19] by ourselves for the case of PFDMS and the analogous poly(ferrocenyl-dimethylgermane) (PFDMG)[20] BCPs, and also by Fukushima and Aida for nanotubes for hexabenzocoronenes with different peripheral substituents.[12c,12h] In this paper we report detailed, proof-of-concept studies of the use of heteroepitaxial growth in 2D for soft materials to create rectangular platelet block comicelles including examples with "patchy" core chemistries.

RESULTS

As a rule of thumb in polymeric systems, a lattice spacing mismatch limit of ca. 15% has been proposed to be a prerequisite for successful heteroepitaxy.[21] Our previous work on the formation of cylindrical multiblock comicelles by heteroepitaxial growth owed its success to the minimal lattice spacing mismatch (ca. 6%)[19] between the core-forming PFDMS and PFDMG blocks of the BCPs involved and presumably the relatively small difference in rates of crystallization.[9f,22] We therefore considered these PFDMS and PFDMG systems to be ideal from the perspective of exploring the extension of heteroepitaxial growth to 2D (Scheme 1).

To investigate the possibility of performing heteroepitaxial growth in 2D, low polydispersity samples of the BCPs $PFDMS_{27}$-*b*-$PDMS_{368}$ and $PFDMG_{24}$-*b*-$PDMS_{264}$ (PDMS = polydimethylsiloxane) and $PFDMS_{25}$-*b*-$P2VP_{500}$ (P2VP = poly(2-vinylpyridine)), and their respective crystalline homopolymers ($PFDMS_{27}$ and $PFDMG_{24}$) (Chart 1) were prepared by living anionic polymerization (for characterization data see Table S1 and Figure S1).[23] $PFDMS_{25}$-*b*-$P2VP_{500}$ BCP was used to form low length-dispersity cylindrical micelles (L_n = 680 nm, L_w = 699 nm, L_w/L_n = 1.03, σ/L_n = 0.15; L_n is the number-average contour length, L_w the weight-average contour length, and σ the standard deviation) by a sequence of spontaneous nucleation, sonication, and seeded growth (Figure S2).[11] These uniform 1D micelles were used as "seed micelles" for the subsequent experiments involving the growth of platelets.

Chart 1. Structures of block copolymers and homopolymers used in this study.

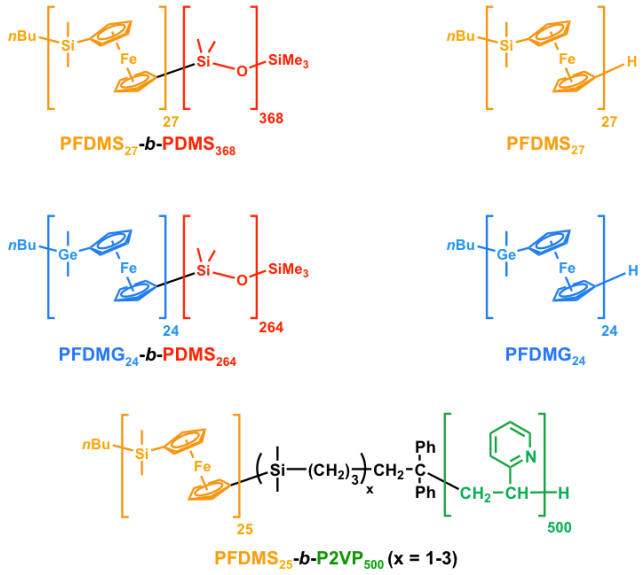

(a). Growth of 2D Platelets with a PFDMG Core from 1D PFDMS-b-P2VP Seeds. First, we targeted the formation of 2D platelets with PFDMG cores using the $PFDMS_{25}$-*b*-$P2VP_{500}$ cylinders as "seeds" (Scheme 1, I). Thus, $PFDMS_{25}$-*b*-$P2VP_{500}$ seeds were dispersed in 1:1 (v/v) ethyl acetate (EtOAc)/*iso*-propanol (*i*-PrOH) and the resulting colloidal solution heated at 45°C for 10 min. A $PFDMG_{24}$-*b*-$PDMS_{264}$/$PFDMG_{24}$ (1:1, w/w) unimer blend in THF was then added with different unimer-to-seed mass ratios (m_{unimer}/m_{seed}). After shaking the solutions for 5 s, samples were annealed at 45°C for an additional 30 min followed by cooling to room temperature (ca. 23°C) and aging overnight for ca. 18 h.

As shown in Figure 1a-f and Figure S3-8, transmission electron microscopy (TEM) analysis of the drop-cast samples of the 2D $PFDMG_{24}$-*b*-$PDMS_{264}$/$PFDMG_{24}$ blend platelets on carbon-coated copper grids revealed a linear relationship between the number average area (A_n) of the platelets, with low area dispersities, and the m_{unimer}/m_{seed} (see plot in Figure 1g).[24] It is noteworthy that the presence of the cylindrical $PFDMS_{25}$-*b*-$P2VP_{500}$ seed micelles is apparent by the darker central region owing to the higher electron scattering by the thicker P2VP coronal layer relative to that arising from the PDMS segments. It is also clear from the dimensions of the newly-formed platelets that growth occurs in a terminal direction, parallel to the long axis of the seed, and also in a lateral direction, perpendicular to the seed's long axis. A control experiment was performed in which the unimer blend was added to EtOAc/*i*-PrOH (1:1, v/v) in the absence of the cylindrical seeds at 45°C (Figure S9). This approach resulted in the formation of polydisperse, poorly defined non-rectangular 2D structures, that were highly aggregated, further confirming the key importance of using seeds in these heteroepitaxial growth experiments.

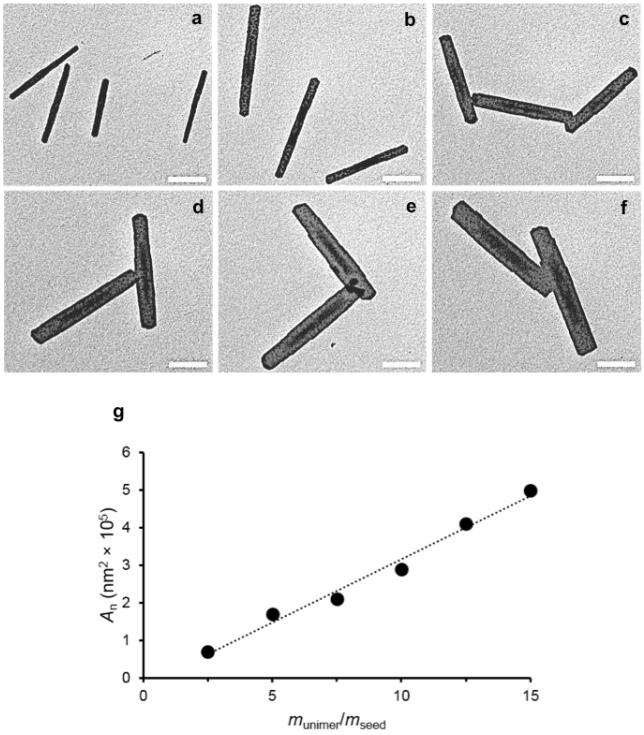

Figure 1. a-f) Bright field TEM micrographs of $PFDMG_{24}$-*b*-$PDMS_{264}$/$PFDMG_{24}$ blend platelets grown from $PFDMS_{25}$-*b*-$P2VP_{500}$ cylinder seeds (L_n = 680 nm, L_w/L_n = 1.03, σ/L_n = 0.15) with m_{unimer}/m_{seed} of 2.5:1 (a), 5:1 (b), 7.5:1 (c), 10:1 (d), 12.5:1 (e), 15:1 (f). Scale bars 500 nm. g) Plot showing the linear dependence of platelet area on m_{unimer}/m_{seed} (for comprehensive characterization of these platelets see Table S2 and Figure S3-8).

Further examination of the platelets shown in Figure 1b (A_n = 1.74 × 10^5 nm², A_w = 1.84 × 10^5 nm², A_w/A_n = 1.06, σ/A_n = 0.24; A_w is weight-average contour area, and σ is the standard deviation) by atomic force microscopy (AFM) revealed a patchy-like surface structure. Thus, the cylindrical seed micelle precursors were observed to have a greater height relative to the newly-formed platelet regions, as shown in the height profile at the center of the platelets perpendicular to their lateral axis (~ 21 nm vs. ~ 11-15 nm) (red line, Figure 2a,b). Intriguingly, the height measured near the termini of cylindrical seeds appeared to have an intermediate value (~18 nm, green line, Figure 2a,b) and a height profile near the terminal edge of the platelets revealed the presence of slightly alternating values of ~11 and ~15 nm (blue line, Figure 2a,b) (for further analysis, see Discussion section, below).

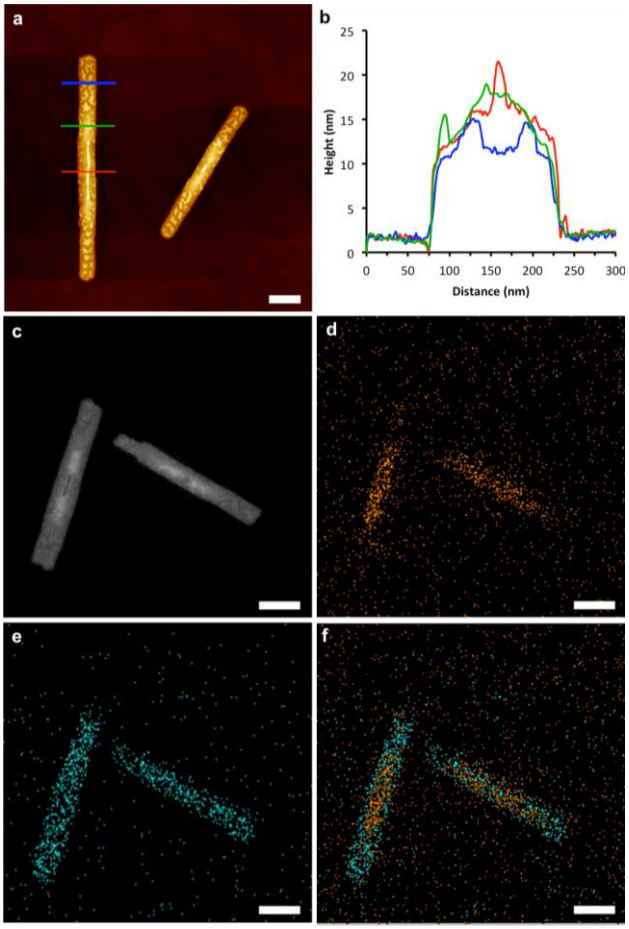

Figure 2. (a) AFM height image and (b) height profile of $PFDMG_{24}$-*b*-$PDMS_{264}$/$PFDMG_{24}$ blend platelets where m_{unimer}/m_{seed} = 5 (A_n = 1.74 × 10^5 nm^2, A_w/A_n = 1.06, σ/A_n = 0.24). (c) Dark field TEM image, (d) STEM-EDX Si-mapping, (e) STEM-EDX Ge-mapping, and (f) overlaid STEM-EDX Si (orange) and Ge (blue) maps of the platelets similar to those shown in (a). Scale bars 250 nm.

By corona-crosslinking of PFDMS-*b*-P2VP/PFDMS platelets using small platinum nanoparticles, we have previously shown that although corona-forming block in the blend platelets covers the whole rectangular platelet surface, it is mainly located in the central regions of the platelet lateral to the seed rather than near the platelet termini.[16] In order to locate the blend components in these well-defined blend platelets formed in the present work we took advantage of the presence of both Ge and Si and, using scanning transmission electron microscopy–energy-dispersive X-ray (STEM–EDX) in elemental mapping mode, directly revealed the locations of these two elements (Figure 2c-f and Figure S10). In these experiments, dark field TEM imaging was used first to locate the platelets on the grid (Figure 2c). In the newly-formed $PFDMG_{24}$-*b*-$PDMS_{264}$/$PFDMG_{24}$ platelet surrounding the seed the only source of Si is the PDMS corona-forming block in the BCP whereas both homopolymer and BCP contribute to the presence of Ge. Si-mapping demonstrated the localization of Si mainly in the central area of the platelets (Figure 2d). This indicates that the BCP is mainly located in this region. On the other hand, as both BCP and homopolymer contain Ge, a more even distribution of this element in the platelet structure is expected and this was observed (Figure 2e). This direct observation of the element distribution for Si and Ge is consistent with our previous finding[16] that in rectangular blend platelets formed by homoepitaxial growth of crystallizable BCP/homopolymer blends, the BCP mainly occupies the central region of the platelet lateral to the seed. The dark field TEM image (Figure 2c) shows a bright region corresponding to higher electron density at each of the seed termini. As noted above, this feature appears to correspond to a region of greater height compared to the remainder of the newly-formed platelet (green line, Figure 2b) and the greater path length would explain the additional degree of electron scattering.

(b). Growth of 2D Platelets with Mixed PFDMS/PFDMG Cores from 1D PFDMS-b-P2VP Seeds. In the aforementioned studies we studied the seeded growth of a blend in which the BCP and homopolymer possessed the same crystallizable core-forming PFDMG block, but different from that of the 1D seeds, where the core was PFDMS. Next, we studied the seeded growth of blends where the two components have a different crystallizable core-forming block. Specifically, we explored whether the $PFDMG_{24}$-*b*-$PDMS_{264}$/$PFDMS_{27}$ or $PFDMS_{27}$-*b*-$PDMS_{368}$/$PFDMG_{24}$ blends would undergo controlled platelet formation in the presence of 1D $PFDMS_{25}$-*b*-$P2VP_{500}$ seeds. Therefore in this case, a lattice mismatch for the core-forming blocks also exists between both of the two blend components rather than solely between the blend and the seed as in the experiments described in Section (a).

We first investigated platelet formation by $PFDMG_{24}$-*b*-$PDMS_{264}$/$PFDMS_{27}$ blends under the same conditions used to generate platelets shown in Figure 2 (Scheme 1, II). This resulted in the formation of well-defined platelets (A_n = 1.93 × 10^5 nm^2, A_w = 1.99 × 10^5 nm^2, A_w/A_n = 1.03, σ/A_n = 0.18) in which their core was composed of a mixture of PFDMS and PFDMG (Figure 3a and Figure S11). Knowing that in these platelets only the BCP is the source of Ge, we then used STEM-EDX elemental mapping to obtain more insight into the blend component distribution in the platelet structure (Figure 3a-d). Interestingly, unlike the case of the $PFDMG_{24}$-*b*-$PDMS_{264}$/$PFDMG_{24}$ platelets above, Ge mapping demonstrated an even distribution of this element, and hence the BCP, in the central and terminal regions of the platelet with no detectable preference with respect to its localization in the central region.

Surprisingly, performing an analogous experiment for $PFDMS_{27}$-*b*-$PDMS_{368}$/$PFDMG_{24}$ blend platelet formation (Scheme 1, III), resulted in the deposition of a precipitate in the vial used for experiment. TEM analysis of the supernatant showed the generation of polydisperse, irregular elongated platelet-type structures (Figure S12). The

inability to form 2D platelet structures in this case can be explained by potential differences in the crystallization rates of PFDMS and PFDMG homopolymers (see Discussion section, below).

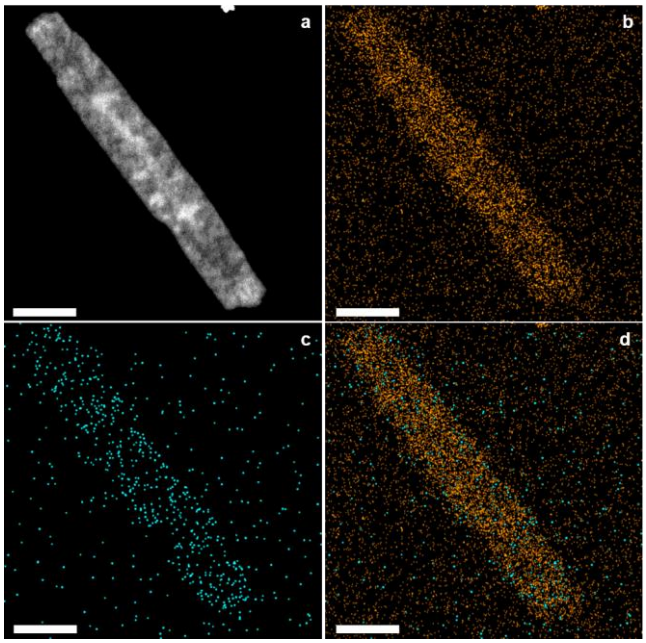

Figure 3. (a) Dark field TEM image, (b) STEM-EDX Si-mapping, (c) STEM-EDX Ge-mapping, and (d) overlaid STEM-EDX Si and Ge maps of the $PFDMG_{24}$-*b*-$PDMS_{264}$/$PFDMS_{27}$ platelets (A_n = 1.93 × 10^5 nm^2, A_w/A_n = 1.03, σ/A_n = 0.18). Scale bars 200 nm.

(c). Growth of 2D Multiblock Platelets with a PFDMS Core from 2D PFDMG-b-PDMS/PFDMG Platelet Precursors. Having successfully accomplished 2D heteroepitaxial growth using 1D seeds, we then targeted the use of the resulting 2D platelets as seed precursors for the subsequent heteroepitaxial growth of a second platelet region on the platelet periphery. To achieve this, we used $PFDMG_{24}$-*b*-$PDMS_{264}$/$PFDMG_{24}$ platelets (A_n = 1.74 × 10^5 nm^2, A_w/A_n = 1.06, σ/A_n = 0.24), shown in Figure 2, as seed micelles for the growth of a $PFDMS_{27}$-*b*-$PDMS_{368}$/$PFDMS_{27}$ outer segment (Scheme 1, IV) under the same, aforementioned conditions. This resulted in the formation of well-defined concentric rectangular platelet block comicelles (A_n = 3.00 × 10^5 nm^2, A_w = 3.14 × 10^5 nm^2, A_w/A_n = 1.05, σ/A_n = 0.22) in which $PFDMG_{24}$-*b*-$PDMS_{264}$/$PFDMG_{24}$ comprised the central platelet block and $PFDMS_{27}$-*b*-$PDMS_{368}$/$PFDMS_{27}$ generated the newly-formed outer region (Figure 4 and Figure S13). As shown in the AFM image in Figure 4a, in the resulting 2D platelet block comicelles the central $PFDMG_{24}$-*b*-$PDMS_{264}$/$PFDMG_{24}$ region preserved its patchy structure observed in Figure 2a. Interestingly, based on the increase in length but virtually unchanged width, the subsequently added $PFDMS_{27}$-*b*-$PDMS_{368}$/$PFDMS_{27}$ blend was mainly deposited in a terminal direction relative to the seed platelet rather than a lateral direction (along the short axis). As with the data obtained for the seed platelets themselves (Figure 2a-b), an AFM height profile at the center of the platelets along their short axis (red line, Figure 4a,b) showed a greater cylindrical seed micelle height relative to the $PFDMG_{24}$-*b*-$PDMS_{264}$/$PFDMG_{24}$ region (~20 nm vs. ~11 nm). A height analysis of a region composed only of the newly-formed $PFDMS_{27}$-*b*-$PDMS_{368}$/$PFDMS_{27}$ platelet region (blue line, Figure 4a,b) revealed a slightly larger value in the center compared to the edge (~12 nm vs ~9 nm).

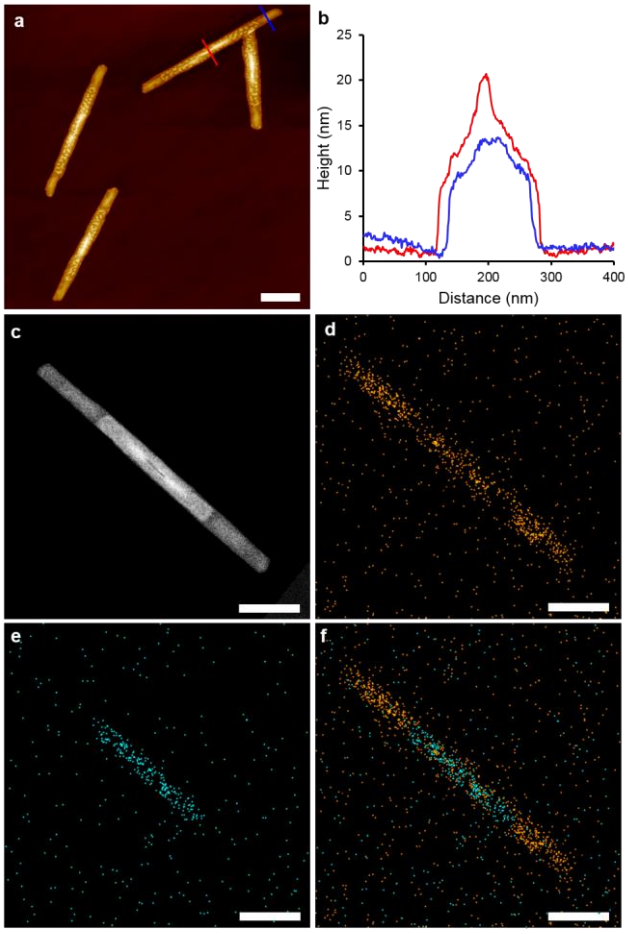

Figure 4. (a) AFM height image and (b) height profile of concentric rectangular platelet block comicelles (A_n = 3.00 × 10^5 nm^2, A_w/A_n = 1.05, σ/A_n = 0.22) prepared through the sequential addition of the $PFDMG_{24}$-b-$PDMS_{264}$/$PFDMG_{24}$ and $PFDMS_{27}$-b-$PDMS_{368}$/$PFDMS_{27}$ blends to $PFDMS_{25}$-b-$P2VP_{500}$ cylindrical seed micelles. (c) Dark field TEM image, (d) STEM-EDX Si-mapping, (e) STEM-EDX Ge-mapping, and (f) overlaid STEM-EDX Si and Ge maps of the platelet block comicelles similar to those shown in (a). Scale bars 500 nm.

In addition, STEM-EDX analysis was employed to further characterize these platelet block comicelles (Figure 4c-f and Figure S13c-f). As shown in Figure 4c, in the dark field TEM image of the resulting block comicelle, the central $PFDMG_{24}$-*b*-$PDMS_{264}$/$PFDMG_{24}$ platelet is easily dis-

tinguishable from the outer region derived from $PFDMS_{27}$-*b*-$PDMS_{368}$/$PFDMS_{27}$ as the former appears brighter than the latter as a result of stronger inelastic electron scattering of Ge. Furthermore, Si-mapping (Figure 4d) showed an interesting pattern in which the two termini of the central block corresponding to the platelet precursor appear sparser in their Si content (Figure 4e) suggesting a higher concentration of Ge in this region. Also, Ge-mapping (Figure 4e) confirmed that this element is confined to the central platelet block.

In order to gain insight into the structures of PFDMG and PFDMS cores in these platelet block comicelles, this sample was analyzed by selected area electron diffraction (SAED). As shown in Figure 5, SAED measurements revealed that the two platelet regions in the platelet block comicelles have identical electron diffraction (ED) patterns with three pairs of diffraction spots, confirming the presence of a single crystalline core with monoclinic symmetry.[18] Based on these measurements, a constant value for the lattice spacing of 6.3 Å was obtained for both the inner region (with a PFDMG core) and the outer region (with a PFDMS core) of the platelet block comicelles. These results are entirely consistent with heteroepitaxial growth (see Discussion section below for further analysis).

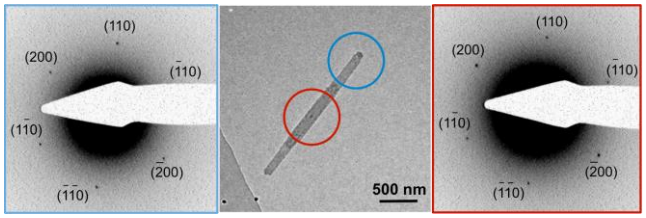

Figure 5. Bright field TEM image and SAED patterns for concentric rectangular platelet block comicelles (A_n = 3.00 × 10^5 nm^2, A_w/A_n = 1.05, σ/A_n = 0.22) prepared through the sequential addition of the $PFDMG_{24}$-b-$PDMS_{264}$/$PFDMG_{24}$ and $PFDMS_{27}$-b-$PDMS_{368}$/$PFDMS_{27}$ blends to $PFDMS_{25}$-b-$P2VP_{500}$ cylindrical seed micelles. ED patterns on left and right correspond to PFDMS- and PFDMG-containing platelet blocks, respectively.[24]

(d). Growth of 2D Platelets with a PFDMG Core from 2D PFDMS-b-PDMS/PFDMS Platelet Precursors. Finally, we investigated whether it was possible to use $PFDMS_{27}$-*b*-$PDMS_{368}$/$PFDMS_{27}$ platelets as seeds for the subsequent growth of an outer $PFDMG_{24}$-*b*-$PDMS_{264}$/$PFDMG_{24}$ region. To explore this possibility, 2D $PFDMS_{27}$-*b*-$PDMS_{368}$/$PFDMS_{27}$ platelets were first prepared using $PFDMS_{25}$-*b*-$P2VP_{500}$ cylindrical seeds (L_n = 680 nm, L_w/L_n = 1.03, σ/L_n = 0.15) under the same conditions as described above (A_n = 1.46 × 10^5 nm^2, A_w = 1.59 × 10^5 nm^2, A_w/A_n = 1.09, σ/A_n = 0.31) (Scheme 1,V and Figure S14). These platelets were then used as seeds for the growth of $PFDMG_{24}$-*b*-$PDMS_{264}$/$PFDMG_{24}$ blocks (Scheme 1,VI). In doing so, well-defined platelet block comicelles with distinct core regions were formed (A_n = 1.08 × 10^6 nm^2, A_w = 1.09 × 10^6 nm^2, A_w/A_n = 1.01, σ/A_n = 0.10) (Figure 6 and Figure S15a,b). Unlike the concentric platelet block comicelles formed by the sequential addition of the $PFDMG_{24}$-*b*-$PDMS_{264}$/$PFDMG_{24}$ and $PFDMS_{27}$-*b*-$PDMS_{368}$/$PFDMS_{27}$ blends to $PFDMS_{25}$-*b*-$P2VP_{500}$ cylindrical seed micelles, the addition of $PFDMG_{24}$-*b*-$PDMS_{264}$/$PFDMG_{24}$ blend unimer to $PFDMS_{27}$-*b*-$PDMS_{368}$/$PFDMS_{27}$ seed platelets resulted in the growth of the newly-formed platelet in both the terminal and lateral directions relative the platelet precursor (Figure 6). As shown in Figure 6a,b, the AFM height profile at the center of the platelet perpendicular to its lateral axis (red line) showed a height for the cylindrical seed micelle of ~16 nm. As for the previously described 2D structures, this protrudes from the surface and on moving toward the lateral edges of the platelet the height initially falls to ~10 nm, corresponding to the $PFDMS_{27}$-*b*-$PDMS_{368}$/$PFDMS_{27}$ central platelet inner region. On reaching the newly-grown outer region derived from the $PFDMG_{24}$-*b*-$PDMS_{264}$/$PFDMG_{24}$ blend a slight increase to ~13 nm was detected. This value then dropped slightly again to ~9 nm in the regions close to the lateral edges of the platelet. In contrast, an AFM height scan of a newly-formed region from $PFDMG_{24}$-*b*-$PDMS_{264}$/$PFDMG_{24}$ near a platelet terminus (blue line, Figure 6a,b) showed, as expected, an absence of the protruding seed, with a value of ~10 nm at the center, and an increase to ~15 nm to the sides. This suggests that the center may be richer in $PFDMG_{24}$ homopolymer with a higher fraction of $PFDMG_{24}$-*b*-$PDMS_{264}$ BCP nearer the platelet edge, where the corona would also make a contribution to the detected height. Consistent with the height profile at the central region of the platelet (red line, Figure 6a,b), the height drops again to ~9 nm at the lateral edges.

The two platelet regions of these block comicelles are clearly distinguishable in their corresponding dark field TEM image (Figure 6c) with the $PFDMS_{27}$-*b*-$PDMS_{368}$/$PFDMS_{27}$ inner region overwhelmingly less bright than that derived from the $PFDMG_{24}$-*b*-$PDMS_{264}$/$PFDMG_{24}$ blend on the platelet periphery. This is once again consistent with the higher electron scattering expected for Ge relative to Si. Using STEM-EDX in elemental mapping mode (Figure 6d-f), an uneven distribution of Si was observed in the platelet block co-micelle structure (Figure 6d) with, as expected, a higher concentration in the central region, reflecting the presence of Si in both the PFDMS core and PDMS corona. In striking contrast, the absence of Ge in the inner platelet block results in a "hollow" pattern for the Ge map (Figure 6e), confirming the presence of distinct core-forming segments in the resulting 2D platelet structures (Figure 6e).

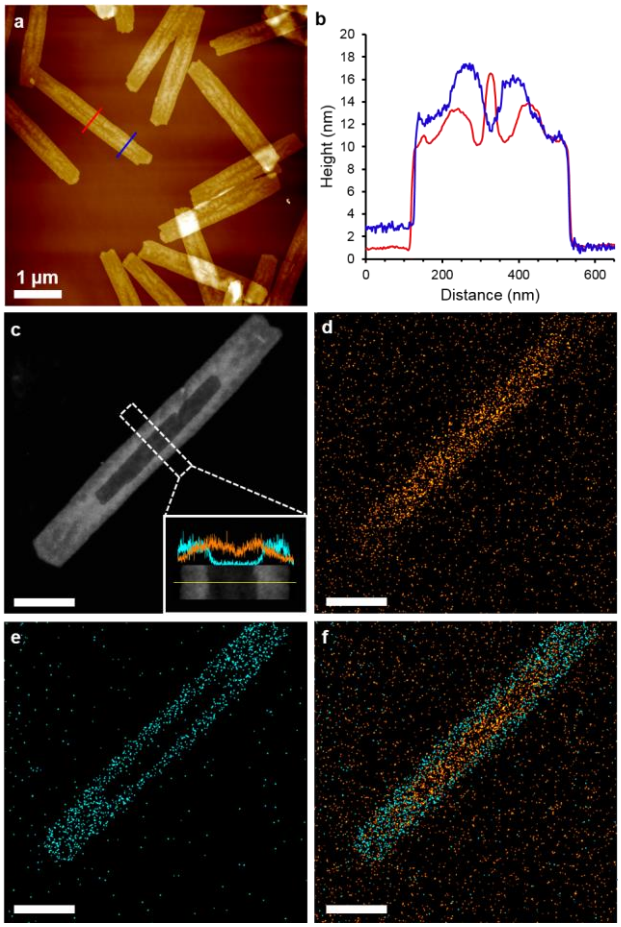

Figure 6. (a) AFM height image and (b) height profile of concentric rectangular platelet block comicelles (A_n = 1.08 × 10^6 nm², A_w/A_n = 1.01, σ/A_n = 0.10) prepared through the sequential addition of the $PFDMS_{27}$-*b*-$PDMS_{368}$/$PFDMS_{27}$ and $PFDMG_{24}$-*b*-$PDMS_{264}$/$PFDMG_{24}$ blends to $PFDMS_{25}$-*b*-$P2VP_{500}$ cylindrical seed micelles. (c) Dark field TEM image, (d) STEM-EDX Si-mapping, (e) STEM-EDX Ge-mapping, and (f) overlaid STEM-EDX Si and Ge maps of the platelet block comicelles similar to those shown in (a). Inset in (c) shows the EDX line analysis across the platelet where the orange and blue lines correspond to Si and Ge analyses, respectively. Scale bars 500 nm (c-f).

DISCUSSION

(i) Formation of Platelets with PFDMG and Mixed PFDMG/PFDMS cores. In the first set of experiments we showed that 2D platelets of controlled dimensions with PFDMG cores (Figure 1a-f) can be formed by the addition of $PFDMG_{35}$-*b*-$PDMS_{315}$/$PFDMG_{35}$ unimer blend to 1D $PFDMS_{25}$-*b*-$P2VP_{500}$ cylinder seeds at 45°C. The formation of these platelets was shown to proceed via a "living" CDSA mechanism where the area (A_n) of the near uniform platelets formed increases linearly with an increase in the m_{unimer}/m_{seed} ratio (Figure 1g). This result clearly shows that uniform platelets can be formed when lattice mismatch exists between the crystallizable segments of the unimer blend components and that of the core-forming block in the 1D seed micelles via heteroepitaxial growth.

An important question to consider is the relative distributions of the BCP and homopolymer components of the blend in the newly-formed regions of the platelet surrounding the seed. Dark field TEM images of $PFDMG_{24}$-*b*-$PDMS_{264}$/$PFDMG_{24}$ platelets revealed an interesting feature whereby regions near the ends of the $PFDMS_{25}$-*b*-$P2VP_{500}$ cylinder seeds are brighter than the platelet termini (Figure 2c). This appears to be a consequence of the greater thickness in this region relative to those further from the seed (Figure 2b). Further insight into the distribution of BCP and homopolymer in the platelet structure was revealed by STEM-EDX measurements (Figure 2d-f). Si-mapping showed that this element is mainly located in the central region of the platelets lateral to the seed but also close to the ends. As the PDMS corona-forming block of the $PFDMG_{24}$-*b*-$PDMS_{264}$ BCP is the only source of Si, this implies that that the BCP is predominantly present in these regions. This suggests that, in this case, the increase in electron scattering observed by dark field TEM in the region close to the seed termini (Figure 2c) is a result of the greater height, and hence path length present, rather than an increased concentration of Ge associated with a larger fraction of homopolymer.

We also examined the possibility of platelet formation using analogous seeded growth of $PFDMG_{24}$-*b*-$PDMS_{264}$/$PFDMS_{27}$ and $PFDMS_{27}$-*b*-$PDMS_{368}$/$PFDMG_{24}$ unimer blends in which lattice mismatch exists between crystallizable segments of each blend component. It was found that only the addition of $PFDMG_{24}$-*b*-$PDMS_{264}$/$PFDMS_{27}$ unimer blend to the $PFDMS_{25}$-*b*-$P2VP_{500}$ cylindrical seeds resulted in the formation of well-defined 2D platelets (Figure 3). In contrast, the use of a $PFDMS_{27}$-*b*-$PDMS_{368}$/$PFDMG_{24}$ unimer blend led to the formation of a precipitate and polydisperse, irregular platelet-type structures remained in the supernatant (Figure S12). The difference in the self-assembly behavior of these two systems is likely to result from the differences in the crystallization rates of PFDMS and PFDMG homopolymers. This may be a consequence of their respective solubilities which influence their relative rates of deposition on the micelle termini. We therefore determined the relative solubility of the two homopolymers $PFDMS_{27}$ and $PFDMG_{24}$ in hexane/cyclohexane as a representative marginal solvent system (1:1 v/v) (see Supporting Information for the detailed experimental procedure). NMR analysis involving the integration of the cyclopentadienyl protons relative to benzene as an internal standard revealed that PFDMS homopolymer is considerably (ca. 45%) more soluble than PFDMG homopolymer in this medium. This difference could result in particularly inefficient co-crystallization of PFDMG homopolymer with $PFDMS_{27}$-*b*-$PDMS_{368}$ BCP and, hence, the formation of ill-defined structures. On the other hand, in the $PFDMG_{24}$-*b*-$PDMS_{264}$/$PFDMS_{27}$ system the PDMS corona-forming block would be expected to slow the deposition of the

PFDMG core-forming block, which in turn could provide sufficient time for co-crystallization with PFDMS homopolymer to form well-defined platelets by heteroepitaxial growth.

Examination of the PFDMG$_{24}$-*b*-PDMS$_{264}$/PFDMS$_{27}$ platelets using STEM-EDX analysis revealed that, unlike the PFDMG$_{24}$-*b*-PDMS$_{264}$/PFDMG$_{24}$ case, the BCP appears to be evenly distributed over the newly-formed platelet region with no preference for its localization in the central region (Figure 3). This result highlights an interesting consequence of the lattice mismatch between the crystallizable core-forming block in the BCP and homopolymer in the blend on the type of the platelet formed. Thus, while using a unimer blend with the same crystalline, core-forming polymer resulted in the preferred localization of the BCP in the central region of the platelet lateral to the seed, using a unimer blend composed of crystalline blocks with a lattice mismatch led to the platelets in which BCP was apparently relatively evenly distributed in their backbone. In the future it will be interesting to explore whether analogous effects are observed when blend combinations are studied with different crystallizable polymers in the future.

(ii) Formation of Concentric Rectangular Platelet Block Comicelles. After successful demonstration of platelet formation via heteroepitaxial growth using 1D seed micelles, generation of well-defined platelet block comicelles using 2D seed precursors was explored. It was found that 2D seed platelets with PFDMG or PFDMS cores were able to form platelet block comicelles upon the addition of PFDMS$_{27}$-*b*-PDMS$_{368}$/PFDMS$_{27}$ or PFDMG$_{24}$-*b*-PDMS$_{264}$/PFDMG$_{24}$ unimer blends, respectively. However, different modes of growth were observed in each case. While the addition of a PFDMS$_{27}$-*b*-PDMS$_{368}$/PFDMS$_{27}$ unimer blend to platelet seeds with PFDMG cores resulted in the growth of the platelets in the terminal rather than lateral direction relative to the seed (Figures 4 and 5), addition of PFDMG$_{24}$-*b*-PDMS$_{264}$/PFDMG$_{24}$ unimer blend to platelet seeds with PFDMS cores led to growth in both directions (Figure 6). This observation is indicative of a significant difference in the growth mechanism in each case and suggests a potentially useful role for the seed platelets in guiding the growth direction of the added blend unimer. Importantly, identical spot-type ED patterns for the two platelet blocks in a block comicelle resulting from the sequential addition of the PFDMG$_{24}$-b-PDMS$_{264}$/PFDMG$_{24}$ and PFDMS$_{27}$-b-PDMS$_{368}$/PFDMS$_{27}$ blends to PFDMS$_{25}$-b-P2VP$_{500}$ cylindrical seed micelles were observed (Figure 5). This corresponded to an identical lattice spacing value of 6.3 Å for each platelet region. We have previously shown that the lattice spacing values for PFDMS and PFDMG homopolymers are 6.3 and 5.9 Å, respectively.[20b] The observation that in these platelet block comicelles a lattice spacing value of 6.3 Å rather than 5.9 Å was obtained for the inner PFDMG-containing platelet region indicated that the central PFDMS$_{25}$-b-P2VP$_{500}$ cylindrical seed micelles dictate the lattice spacing for the added PFDMG-based blend. This is indicative of a heteroepitaxial growth mechanism in 2D. This lattice spacing is then also transferred to the region subsequently formed by the PFDMS-based blend, as expected.[24]

SUMMARY

We have demonstrated that living CDSA of blends of PFDMS- or PFDMG-containing BCPs together with the corresponding homopolymers allows the formation of well-defined platelet and platelet block comicelles using either 1D cylindrical or 2D platelet seed micelles via a heteroepitaxial growth mechanism. Platelet block comicelles with alternating PFDMS and PFDMG cores of varying sequence were constructed. It was shown that the type of seed platelet plays an important role in the growth direction of the added block. Thus, when PFDMG$_{24}$-*b*-PDMS$_{264}$/PFDMG$_{24}$ platelets were used as seeds, the added PFDMS$_{27}$-*b*-PDMS$_{368}$/PFDMS$_{27}$ unimer tended to mainly grow terminal to the seed micelles, whereas the use of PFDMS$_{27}$-*b*-PDMS$_{368}$/PFDMS$_{27}$ seed platelets directed the growth of the added PFDMG$_{24}$-*b*-PDMS$_{264}$/PFDMG$_{24}$ unimer in both terminal and lateral directions. SAED analysis of platelet block comicelles formed by the sequential addition of the PFDMG$_{24}$-b-PDMS$_{264}$/PFDMG$_{24}$ and PFDMS$_{27}$-b-PDMS$_{368}$/PFDMS$_{27}$ blends to PFDMS$_{25}$-b-P2VP$_{500}$ cylindrical seed micelles indicated that the lattice structure of the inner PFDMG-containing platelet block is governed by the lattice spacing of the central PFDMS-containing cylindrical seed micelle, as expected for a heteroepitaxial growth mechanism.

The factors influencing the relative locations of the added BCP and homopolymer blend components in the resulting 2D platelets are not yet completely resolved. Based on STEM-EDX studies, in the PFDMG$_{24}$-*b*-PDMS$_{264}$/PFDMG$_{24}$ platelets, where the BCP and homopolymer share the same type of crystalline polymer, the BCP was found to mainly localize in the central region. On the other hand, in the PFDMG$_{24}$-*b*-PDMS$_{264}$/PFDMS$_{27}$ system, where the two crystalline segments are different, BCPs were approximately evenly distributed in the resulting platelets.

Further studies to elucidate the growth mechanism for these and related 2D materials are clearly needed and are currently underway. It appears likely that, in the case of cylindrical seeds, initial growth occurs at the seed termini and the component to deposit first will be dictated by a combination of relative solubility and crystallization rate. Based on our results on seeded homoepitaxial growth of BCP/homopolymer blends reported earlier,[16] it appears that following an initial addition to the seed termini, subsequent encapsulation of the seed to afford a rectangular platelet must be rapid as monitoring of the growth indicates that terminal and lateral growth are almost simultaneous. We are also investigating potential applications of the structures. In particular, transposing this approach to

blends containing other crystalline core-forming blocks such as π-conjugated materials, which also undergo living CDSA,[25] is of considerable interest and may allow the creation of 2D heterojunctions and other functional assemblies.

ASSOCIATED CONTENT

Supporting Information

Experimental procedures and additional data. This material is available free of charge via the Internet at http://pubs.acs.org.

AUTHOR INFORMATION

Corresponding Author

*To whom correspondence should be addressed:
ian.manners@bristol.ac.uk

ORCID

Ali Nazemi: 0000-0002-6504-582X

Mitchell A. Winnik: 0000-0002-2673-2141

Ian Manners: 0000-0002-3794-967X

Author Contributions

§X.H. and L.R.M. contributed equally.

Notes

The authors declare no competing financial interest.

ACKNOWLEDGMENT

A.N. and X.H. are grateful to the European Union for Marie Curie Fellowships. L.R.M thanks EPSRC for support. PeakForce atomic force microscopy was carried out in the Chemical Imaging Facility, University of Bristol with equipment funded by EPSRC. TEM studies were carried out in the Chemistry Imaging Facility at University of Bristol with equipment funded by UoB and EPSRC.

Keywords: block copolymers • crystallization-driven self-assembly • two-dimensional • heteroepitaxial growth • block comicelles

REFERENCES

(1) a) Boott, C. E.; Nazemi, A.; Manners, I., *Angew. Chem., Int. Ed.* **2015**, *54*, 13876; b) Zhuang, X.; Mai, Y.; Wu, D.; Zhang, F.; Feng, X., *Adv. Mater.* **2015**, *27*, 403.

(2) a) Li, B.; Li, C. Y., *J. Am. Chem. Soc.* **2007**, *129*, 12; b) Dong, B.; Zhou, T.; Zhang, H.; Li, C. Y., *ACS Nano* **2013**, *7*, 5192.

(3) Li, B.; Wang, B. B.; Ferrier, R. C. M.; Li, C. Y., *Macromolecules* **2009**, *42*, 9394.

(4) Zhang, L. F.; Eisenberg, A., *Science* **1995**, *268*, 1728.

(5) Pochan, D. J.; Chen, Z. Y.; Cui, H. G.; Hales, K.; Qi, K.; Wooley, K. L., *Science* **2004**, *306*, 94.

(6) Koide, A.; Kishimura, A.; Osada, K.; Jang, W.-D.; Yamasaki, Y.; Kataoka, K., *J. Am. Chem. Soc.* **2006**, *128*, 5988.

(7) Cui, H.; Chen, Z.; Zhong, S.; Wooley, K. L.; Pochan, D. J., *Science* **2007**, *317*, 647.

(8) For early studies on platelets with crystalline cores see: a) Lotz, B.; Kovacs, A. J., *Kolloid Z. Z. Polym.* **1966**, *209*, 97 ; b) Lotz, B.; Kovacs, A. J.; Bassett, G. A.; Keller, A., *Kolloid Z. Z. Polym.* **1966**, *209*, 115; c) Vilgis, T.; Halperin, A., *Macromolecules* **1991**, *24*, 2090; d) Gast, A. P.; Vinson, P. K.; Coganfarinas, K. A., *Macromolecules* **1993**, *26*, 1774.

(9) For representative recent work on platelets with crystalline cores see: a) Chen, W. Y.; Li, C. Y.; Zheng, J. X.; Huang, P.; Zhu, L.; Ge, Q.; Quirk, R. P.; Lotz, B.; Deng, L.; Wu, C.; Thomas, E. L.; Cheng, S. Z. D., *Macromolecules* **2004**, *37*, 5292; b) Zheng, J. X.; Xiong, H.; Chen, W. Y.; Lee, K.; Van Horn, R. M.; Quirk, R. P.; Lotz, B.; Thomas, E. L.; Shi, A.-C.; Cheng, S. Z. D., *Macromolecules* **2006**, *39*, 641; c) Wang, J.; Zhu, W.; Peng, B.; Chen, Y. M., *Polymer* **2013**, *54*, 6760; d) Su, M.; Huang, H. Y.; Ma, X. J.; Wang, Q.; Su, Z. H., *Macromol. Rapid Commun.* **2013**, *34*, 1067; e) Cao, L.; Manners, I.; Winnik, M. A., *Macromolecules* **2002**, *35*, 8258; f) Mohd Yusoff, S. F.; Hsiao, M.-S.; Schacher, F. H.; Winnik, M. A.; Manners, I., *Macromolecules* **2012**, *45*, 3883; g) Wang, Z.; Cao, Y.; Song, J.; Xie, Z.; Wang, Y., *Langmuir* **2016**, *32*, 9633; h) Wu, J.; Weng, L.-T.; Qin, W.; Liang, G.; Tang, B. Z., *ACS Macro Lett.* **2015**, *4*, 593; i) Li, Z.; Liu, R.; Mai, B.; Wang, W.; Wu, Q.; Liang, G.; Gao, H.; Zhu, F., *Polymer* **2013**, *54*, 1663.

(10) a) Massey, J. A.; Temple, K.; Cao, L.; Rharbi, Y.; Raez, J.; Winnik, M. A.; Manners, I., *J. Am. Chem. Soc.* **2000**, *122*, 11577; b) Du, Z.-X.; Xu, J.-T.; Fan, Z.-Q., *Macromolecules* **2007**, *40*, 7633; c) Fairley, N.; Hoang, B.; Allen, C., *Biomacromolecules* **2008**, *9*, 2283; d) Fujiwara, T.; Miyamoto, M.; Kimura, Y.; Iwata, T.; Doi, Y., *Macromolecules* **2001**, *34*, 4043; e) Pitto-Barry, A.; Kirby, N.; Dove, A. P.; O'Reilly, R. K., *Polym. Chem.* **2014**, *5*, 1427; f) Mihut, A. M.; Drechsler, M.; Moller, M.; Ballauff, M., *Macromol. Rapid Commun.* **2010**, *31*, 449; g) Lee, C.-U.; Smart, T. P.; Guo, L.; Epps, T. H.; Zhang, D., *Macromolecules* **2011**, *44*, 9574; h) Wurm, F.; Hilf, S.; Frey, H., *Chem. Eur. J.* **2009**, *15*, 9068; i) Brubaker, C. E.; Velluto, D.; Demurtas, D.; Phelps, E. A.; Hubbell, J. A., *ACS Nano* **2015**, *9*, 6872.

(11) a) Wang, X.; Guerin, G.; Wang, H.; Wang, Y.; Manners, I.; Winnik, M. A., *Science* **2007**, *317*, 644; b) Gilroy, J. B.; Gädt, T.; Whittell, G. R.; Chabanne, L.; Mitchels, J. M.; Richardson, R. M.; Winnik, M. A.; Manners, I., *Nature Chem.* **2010**, *2*, 566; c) Hudson, Z. M.; Lunn, D. J.; Winnik, M. A.; Manners, I., *Nat. Commun.* **2014**, *5*, 3882; d) Finnegan, J. R.; Lunn, D. J.; Gould, O. E. C.; Hudson, Z. M.; Whittell, G. R.; Winnik, M. A.; Manners, I., *J. Am. Chem. Soc.* **2014**, *136*, 13835.

(12) a) Petzetakis, N.; Dove, A. P.; O'Reilly, R. K., *Chem. Sci.* **2011**, *2*, 955; b) Schmelz, J.; Schedl, A. E.; Steinlein, C.; Manners, I.; Schmalz, H., *J. Am. Chem. Soc.* **2012**, *134*, 14217; c) Zhang, W.; Jin, W.; Fukushima, T.; Saeki, A.; Seki, S.; Aida, T., *Science* **2011**, *334*, 340; d) Ogi, S.; Sugiyasu, K.; Manna, S.; Samitsu, S.; Takeuchi, M., *Nature Chem.* **2014**, *6*, 188; e) Robinson, M. E.; Lunn, D. J.; Nazemi, A.; Whittell, G. R.; De Cola, L.; Manners, I., *Chem. Commun.* **2015**, *51*, 15921; f) Bu, L.; Dawson, T. J.; Hayward, R. C., *ACS Nano* **2015**, *9*, 1878; g) Ogi, S.; Stepanenko, V.; Sugiyasu, K.; Takeuchi, M.; Würthner, F., *J. Am. Chem. Soc.* **2015**, *137*, 3300; h) Zhang, W.; Jin, W.; Fukushima, T.; Mori, T.; Aida, T., *J. Am. Chem. Soc.* **2015**, *137*, 13792; i) Schmelz, J.; Karg, M.; Hellweg, T.; Schmalz, H., *ACS Nano* **2011**, *5*, 9523; j) Sun, L.; Pitto-Barry, A.; Kirby, N.; Schiller, T. L.; Sanchez, A. M.; Dyson, M. A.; Sloan, J.; Wilson, N. R.; O'Reilly, R. K.; Dove, A. P., *Nat. Commun.* **2014**, *5*; k) Ma, X. J.; Zhang, Y. B.; Zhang, Y. F.; Liu, Y.; Che, Y. K.; Zhao, J. C., *Angew. Chem., Int. Ed.* **2016**, *55*, 9538; l) Pal, A.; Malakoutikhah, M.; Leonetti, G.; Tezcan, M.; Colomb-Delsuc, M.; Nguyen, V. D.; van der Gucht, J.; Otto, S., *Angew. Chem., Int. Ed.* **2015**, *54*, 7852.

(13) Hailes, R. L. N.; Oliver, A. M.; Gwyther, J.; Whittell, G. R.; Manners, I., *Chem. Soc. Rev.* **2016**, *45*, 5358.
(14) Hudson, Z. M.; Boott, C. E.; Robinson, M. E.; Rupar, P. A.; Winnik, M. A.; Manners, I., *Nature Chem.* **2014**, *6*, 893.
(15) Yu, B.; Jiang, X.; Yin, J., *Macromolecules* **2014**, *47*, 4761.
(16) Qiu, H.; Boott, C. E.; Gould, O. E. C.; Harniman, R. L.; Miles, M. J.; Webb, S. E. D.; Winnik, M. A.; Manners, I., *Science* **2016**, *352*, 697.
(17) In the absence of seeds blends of crystallizable BCPs and their corresponding homopolymers, such as PCL-b-PEO with PCL, and poly(ferrocenyldimethylsilane) (PFDMS) with PFDMS-b-PI (PI = polyisoprene), has been shown to result in the formation of polydis- perse 2D platelet structures. See: (a) Rizis, G.; van deVen, T. G. M.; Eisenberg, A., *Angew. Chem., Int. Ed.* **2014**, *53*, 9000; (b) Cambridge, G.; Gonzalez-Alvarez, M. J.; Guerin, G.; Manners, I.; Winnik, M. A., *Macromolecules* **2015**, *48*, 707. In addition, the co-assembly or "blending" of different BCPs has been shown to provide a useful route to conventional and also more complex morphologies such as disk-sphere or disk-cylinder hybrid micelles: see, (c) Wright, D. B.; Patterson, J. P.; Pitto-Barry, A.; Lu, A.; Kirby, N.; Gianneschi, N. C.; Chassenieux, C.; Colombani, O.; O'Reilly, R. K., *Macromolecules* **2015**, *48*, 6516; (d) Zhu, J.; Zhang, S.; Zhang, K.; Wang, X.; Mays, J. W.; Wooley, K. L.; Pochan, D. J., *Nat. Commun.* **2013**, *4*, 2297.
(18) a) Gilroy, J. B.; Rupar, P. A.; Whittell, G. R.; Chabanne, L.; Terrill, N. J.; Winnik, M. A.; Manners, I.; Richardson, R. M., *J. Am. Chem. Soc.* **2011**, *133*, 17056; b) Hsiao, M.-S.; Yusoff, S. F. M.; Winnik, M. A.; Manners, I., *Macromolecules* **2014**, *47*, 2361.
(19) Gädt, T.; Ieong, N. S.; Cambridge, G.; Winnik, M. A.; Manners, I., *Nat. Mater.* **2009**, *8*, 144.
(20) a) Foucher, D. A.; Edwards, M.; Burrow, R. A.; Lough, A. J.; Manners, I., *Organometallics* **1994**, *13*, 4959; b) Ieong, N. S.; Manners, I., *Macromol. Chem. Phys.* **2009**, *210*, 1080.
(21) a) Wittmann, J. C.; Lotz, B., *J. Polym. Sci., Part B: Polym. Phys.* **1981**, *19*, 1837; b) Wittmann, J. C.; Hodge, A. M.; Lotz, B., *J. Polym. Sci., Part B: Polym. Phys.* **1983**, *21*, 2495.
(22) Gädt, T.; Schacher, F. H.; McGrath, N.; Winnik, M. A.; Manners, I., *Macromolecules* **2011**, *44*, 3777.
(23) a) Ni, Y.; Rulkens, R.; Manners, I., *J. Am. Chem. Soc.* **1996**, *118*, 4102; b) Peckham, T. J.; Massey, J. A.; Edwards, M.; Manners, I.; Foucher, D. A., *Macromolecules* **1996**, *29*, 2396; c) Wang, H.; Winnik, M. A.; Manners, I., *Macromolecules* **2007**, *40*, 3784.
(24) To date, well-defined PFDMG-based cylindrical seeds have not been prepared because spontaneous nucleation results in cylindrical micelles with defect-rich cores (see ref. 19). For this reason, the reverse experiment, involving heteroepitaxial growth in 2D by the addition of $PFDMS_{27}$-*b*-$PDMS_{368}$/$PFDMS_{27}$ blend unimer to PFDMG-based cylindrical seeds, could not be performed.
(25) a) Gwyther, J.; Gilroy, J. B.; Rupar, P. A.; Lunn, D. J.; Kynaston, E.; Patra, S. K.; Whittell, G. R.; Winnik, M. A.; Manners, I., *Chem. Eur. J.* **2013**, *19*, 9186; b) Qian, J.; Li, X.; Lunn, D. J.; Gwyther, J.; Hudson, Z. M.; Kynaston, E.; Rupar, P. A.; Winnik, M. A.; Manners, I., *J. Am. Chem. Soc.* **2014**, *136*, 4121.

. Table of Content